# Journal of Materials Chemistry B

Accepted Manuscript






ROYAL SOCIETY OF CHEMISTRY

www.rsc.org/materialsB

Journal Name

RSCPublishing

ARTICLE

# Polypyrrole-paraphenolsulfonic Acid/Tape Artificial Muscle as a Tool to Clarify Biomimetic Driven Reactions and Ionic Exchanges

Masaki Fuchiwaki[a],[b] and Toribio F. Otero[b]

Cite this: DOI: 10.1039/x0xx00000x

Received 00th January 2012,
Accepted 00th January 2012

DOI: 10.1039/x0xx00000x

www.rsc.org/

Thick films of the polypyrrole-paraphenolsulfonic acid (PPy-HpPS) blend were electrogenerated on stainless steel plates. The self-supported films, once peeled off from the metal, were electrochemically characterized in aqueous solutions of NaCl and $NaPF_6$. The Na, Cl, P, S and F content of films, after attaining a different oxidation state, were determined by EDX. The bending movements of bilayer (PPy-HpPS)/tape artificial muscle were video recorded during potential sweeps in both solutions allowing the translation of the prevalent ionic exchanges driven by the biomimetic reactions into macroscopic movements. Ionic exchanges between the film and the solution, biomimetic structural processes in the film, driving prevalent electrochemical reactions and film compositions related to each of different structural potential domains defined by coulovoltammetric results were clarified. In $NaPF_6$ solutions a prevalent exchange of anion exists: the film swells by oxidation and shrinks by reduction. In NaCl solutions prevailing exchange of cations or anions occur in different potential ranges. Reactions related to the HpPS content play important roles at the more cathodic and more anodic overpotentials. Described methodology could be translated to biological reactions including reactive biopolymers.

## 1 Introduction

Films of conducting polymers in aqueous solutions constitute the simplest material model (reactive polymer chains, ions and water) of the reactive intracellular matrix (ICM) which reactions originate biological functions.[1,2] The shift by several orders of magnitudes of the ionic composition gives unprecedented chemical materials. The composition dependent properties (volume, color, stored charge, porosity, chemical storage or wettability, among others) also shift, in a reversible way, under electrochemical control.[1] Those faradaic properties originate devices driven by the material reaction (chemical, or reactive, devices) as: artificial muscles, full organic batteries and supercapacitors, smart windows-mirrors or screens, smart membranes, electron-ion transducers, artificial glands or artificial chemical synapses, among others.[3-5] Our group has empirically demonstrated and theoretically described that any physical or chemical variable acting on the reaction rate will be sensed by the device while working.[6-8] New dual sensing-actuating devices as haptic artificial muscles, mimicking brain-muscles feedback communication, are being developed. Additionally, the reaction kinetic magnitudes (reaction coefficient, activation energy and reaction orders) include structural information: the Chemical kinetics becomes Structural Chemical Kinetics,[9] envisaging predictive chemical models for biochemical reactions and biological functions or miss-functions.[10,11]

Both, reactive properties and reactive devices are based on ionic and aqueous exchanges between the conducting polymer film and the electrolyte driven by the electrochemical reaction. Different methodologies are being used trying to quantify the key aqueous[11-22] and ionic exchanges per unit of charge: using bending artificial muscles as practical tools,[12,13] by analyzing the electrochemical impedance responses from coated electrodes,[17-21] or through theoretical approaches from oligomeric films in electrolytes by using molecular dynamic simulations.[14-16]

The most popular, from 20 years ago, is the Electrochemical Quartz Crystal Microbalance (EQCM).[23-30] When applied to polypyrole films electrogenerated from aqueous solutions of small anions, also checked in presence of small anions, an exchange of anions (ingress/expel by oxidation/reduction, respectively) is claimed to occur in a large anodic potential range. At cathodic potentials the exchange of cations (ingress/expel by reduction/oxidation, respectively) is claimed. Recently by changing the voltammetric response from the QCM electrode to coulovoltammetric responses a significant irreversible charge (attributed to the hydrogen evolution at the metal/polymer interface) was detected, overlapping the

potential region of the claimed cation exchange.[31] When the metal/polymer interface was eliminated by using self-supported polypyrrole films or polymer/tape bilayer artificial muscles, in both cases the electric contact through the metal clamp being located far away from the solution, has corroborated the absence of both processes: the film expansion (and the concomitant bending movement) due to the claimed cation's exchange and the irreversible reaction.[32] The absence of cations in deep reduced PPy films at high cathodic potentials was corroborated by EDX analysis.[33]

It is well known that most of the polymeric blend materials of basic conducting polymers with: polyanions, poly-acids or large organic anions, experience a prevalent exchange of cations during redox reactions.[34-39]

The open question now is which kind of ionic exchange occurs if we select an organic acid having an intermediate molecular size (between polystyrene sulphonic and acetic acid): paraphenolsulfonic acid (HpPS) to generate a PPy blend during its subsequent control in different electrolytes. Here we will present the electrogeneration (Py electropolymerization plus HpPS adsorption)[2] of the new polypyrrole blend (PPy-HpPS). The self-supported blend film and the PPy-HpPS/tape artificial muscle will be studied in aqueous solutions of NaCl or $NaPF_6$ video-recording the driven bending movements of the bilayer. The composition of the PPy-HpPS film under different oxidation and reductions states attained in each electrolyte will be analysed by XPS. The attained information will be used to try to clarify: electrochemical reactions, electrochemical driven ionic exchanges between the film and each electrolyte and electrochemical driven structural processes taking place in the film at different potential ranges.

## 2 Experimental

### 2.1 Chemicals

Pyrrole (Fluka) was purified by distillation under vacuum using a diaphragm vacuum pump (MZ 2C, SCHOTT_) and stored in a refrigerator at -15 °C. The paraphenolsulfonic acid (HpPS), Figure 1(a), solution (Aldrich) was used as received. Ultrapure water from Millipore Milli-Q equipment was used.

### 2.2 Film preparations

The PPy-HpPS films were electrogenerated at 0 °C in a one-compartment electrochemical cell using 50 mL of 0.1M HpPS and 0.15M pyrrole aqueous solutions. The temperature was controlled by using a Julabo T25 cryostat/thermostat having a precision of 0.1 °C. The working electrode was an AISI316 stainless steel plate, having a thickness of 1.24 mm and a surface area of 20 × 50 mm. The PPy-HpPS film was electrogenerated on both sides of the immersed part (20 × 15 mm) of the stainless steel plate. Two stainless steel counter electrodes having a surface area of 20 × 50 mm were located symmetrically and parallel, at 1cm, at both sides of the stainless steel working electrode to obtain a uniform electric field. A standard Ag/AgCl (3M KCl) electrode from Metrohm® was used as the reference electrode.

The PPy-HpPS film was electro-generated by applying a constant anodic current density of 0.5 mA $cm^{-2}$ for 7200 seconds through the working stainless steel plate. Figure 1(b) shows the evolution of the working electrode potential during

a b

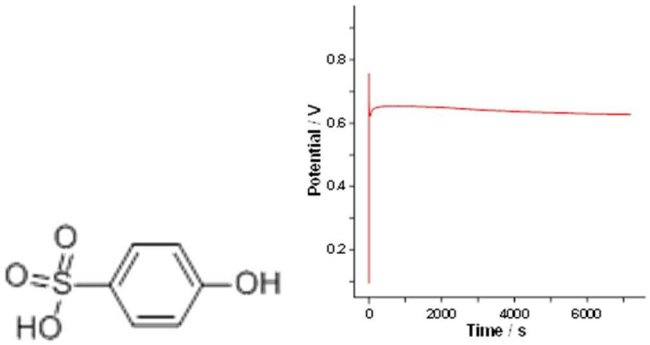


**Fig. 1** (a) 4-Hydroxybenzenesulfonic acid (para-phenolsulfonic acid, HpPS) solution (b) Evolution of the potential during the electropolymerization times by applying a constant anodic current density of 0.5 mA cm-2 for 7200 seconds through the stainless steel working electrode.

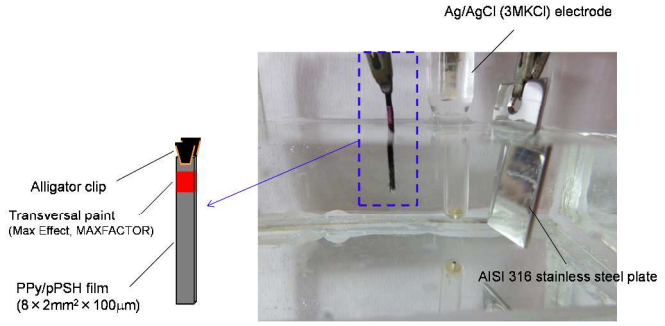


**Fig. 2** Three electrodes electrochemical cell: Freestanding PPy-HpPS film electrode (electric contact through the alligator clip and the dry PPy-HpPS film fraction, transversal paint strip to avoid the electrolyte capillarity and PPy-HpPS film fraction immersed in the electrolyte), AISI 316 Stainless steel counter electrode, Ag/AgCl reference electrode.

the electropolymerization time. A black polypyrrole film is formed on each electrode side during this time. The potential of the working electrodes during the electrogeneration of the polymer film keeps almost constant around 0.65 mV. The overall charge consumed during the film electropolymerization was 4.8 C. Once the working electrode was coated, the polypyrrole material coating the electrode borders was scraped. After peeling off from the working electrode the two pPy-HpPS films were rinsed with water and dried in air at room temperature. Every film was then cut getting longitudinal strips having similar dimensions.

### 2.3 Self-supported electrode films

The dimensions (measured using a COMECTA electronic digital micrometer) of each of the PPy-HpPS dry strips were 8 × 2 mm, having a thickness of 100 μm and weighing 0.83 ±

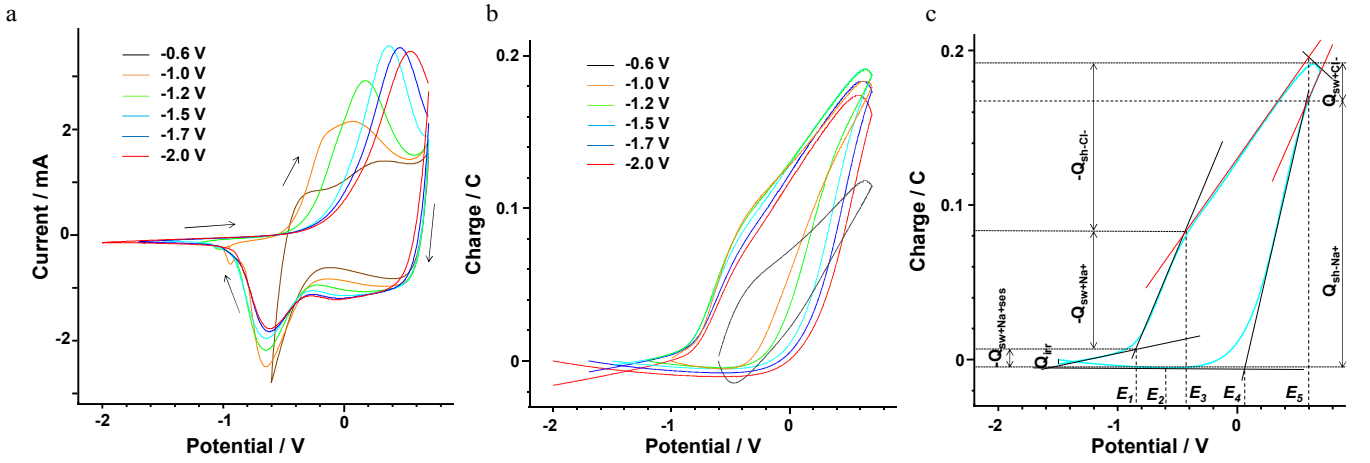


**Fig. 3** (a) Stationary voltamnograms using a self-supported PPy-HpPS film electrode from different cathodic potential limits ranging from -0.6 V to -2.0 V and the same anodic potential limit of 0.7 V, at 10 mV $s^{-1}$ in 0.5 M NaCl aqueous solution. (b) Coulovoltammetric responses obtained by integration of the voltammograms from figure 3a. (c) Coulovoltammetric response between -1.5 V, and 0.7 V, showing abrupt slope variations related to abrupt reaction rates changes (dQ/dt =dn/dt, were n=Q/F is the number of exchanged electrons and ions and F the Faraday constant) due to structural transitions inside the film driven by the reactions. Each of the abrupt slope changes indicates a potential characteristic of a structural/reaction change: $E_1$, $E_2$, $E_3$, $E_4$, $E_5$; the charge difference between two characteristic potentials correspond to the charge of the concomitant structural process.

0.01 mg. In order to avoid the contact between the metal clip (used for the electrical contact) and the electrolyte by capillarity the dry films were coated on both sides with a transversal paint strip (Max Effect, MAXFACTOR) from 2.0 mm to 5.0 mm of the upper border (Figure 2a and 2b). The top 2.0 mm of free paint film allows the electronic contact with the working electrode exit of the potentiostat/galvanostat through the alligator clip. The electrode film was immersed in the aqueous electrolyte, the meniscus remaining below the transversal paint strip, for its subsequent electrochemical characterization.

### 2.4 Electrochemical behaviour of the self-supported PPy-HpPS film.

The electrochemical characterization was performed at room temperature (22±1 °C) using an Autolab PGSTAT-100 potentiostat/galvanostat controlled by a personal computer through a GPES (General Purpose Electrochemical System) electrochemical software. All the experiments were performed in a one-compartment electrochemical cell. One of the self-supported films above prepared was used as the working electrode. An AISI 316 stainless steel plate was used as the counter-electrode and the standard Ag/AgCl (3MKCl) was the reference electrode.

## 3 Results and discussion

### 3.1 Stationary Voltammetric Responses from Different Cathodic Potential Limits

strong cathodic potential shift parallel to the anodic potential shift above described for the main anodic maximum.

As a partial conclusion the voltammetric responses are deeply influenced by the strong structural changes suffered by the polymer at more cathodic potentials than the main voltammetric cathodic maximum.

The PPy-HpPS film was submitted to consecutive voltammetric cycles between -0.4 V and 0.7 V at a scan rate of 10 mV $s^{-1}$, at room temperature in 0.5 M NaCl aqueous solution. After 32 consecutive potential cycles any structural memory from the material was erased, getting stationary voltammetric responses: the consecutive voltammograms overlap.

Figures 3(a) show the stationary cyclic voltammetric (CV) responses obtained from the self-supported films (after stabilization) from different cathodic potential limits ranging between -0.6 V and -2.0 V up to the same anodic potential limit of 0.7 V every time, keeping constant the rest of the experimental conditions above described. The beginning of the film oxidation shifts to rising anodic potentials when the polymer was reduced until increasing cathodic potential limits. Those are characteristic facts of the presence of a more energetically stable reduced state, as those described by the Electrochemically Stimulated Conformational Relaxation (ESCR) model, at rising cathodic potential limits.[40,41] The subsequent oxidation starts by nucleation-relaxation at rising anodic potentials: under constant chemical and thermal conditions a higher energy (the anodic overpotential) is required to relax the rising stable structures attained by reduction at more cathodic overpotentials. The fact that the oxidation starts by nucleation-relaxation will be checked later on, from the chronoamperometric responses of the film submitted to potential steps.

The second important aspect is that the reduction branches include two reduction processes (current maxima at -0.3 and -0.8V). The first reduction maximum from fig 3a presents a

### 3.2 Stationary coulovoltammetric responses: reversible and irreversible reaction charges

As usual the voltammetric responses seem to include only reversible redox processes taking place in the film. The

presence of structural changes in films of conducting polymers driven by the electrochemical reactions, altogether the possible presence of irreversible reactions are better characterized and visualized by integration of the voltammetric responses to coulovoltammetric responses.[24] From figures 3a the concomitant coulovoltammetric responses, figures 3b, were obtained: oxidation reactions give a positive charge increment along the coulovoltammogram and reduction reactions give negative charge increment.

Whatever the cathodic potential limit a continuous variation of the charge, indicating the presence of faradaic reactions, is present in the full potential range. Closed coulovoltammetric responses were obtained for cathodic potential limits lower than -1.0V: the oxidation charge equals the reduction charge indicating that only reversible film oxidation and reduction reactions are there involved. For more cathodic potential limits than -1.0V every coulovoltammogram shows (Fig. 3b) two different parts, a closed loop and an open part. The closed loop quantifies the charge (maximum to minimum range) involved in the reversible film oxidation/reduction. The negative charge increment between the starting point and the end point of the open part is the charge consumed by an irreversible reduction ($Q_{irr}$, Fig 3c) reaction overlapping the film reduction.[31,32] The presence of the acid (HpPS) in the film seems to catalyse the slow discharge of the water protons.[32] This reaction is slow because doesn't produce any significant increase of the current on the voltammetric responses (Figures 3a) and it is full inhibited in polypyrrole films with small inorganic anions up to more cathodic potential limits than -3V from aqueous solutions.[31] Table 1 presents the charges involved in figure 3b for the reversible film oxidation/reduction reactions and for the irreversible reduction process as a function of the cathodic potential limit. The film redox component of the charge increases with the cathodic potential limit up to -1.2 to -1.5V and then decreases for more cathodic potential limits. According with the structural interpretation of the electrochemical responses from conducting polymers this charge evolution is a results of two crossing effects: the increase of the reduction (and structural stabilization) charge with the cathodic potential limit and the decrease of the oxidation charge during the subsequent anodic sweep due to the anodic structural shift of the oxidation-nucleation maximum (Figures 3a and 3b). All the observed changes, potential shifts and charge evolution are reversed going back to that corresponding to any previous potential limit after a few consecutive voltammograms: the structural memory is erased and the same specific response observed on figure 3a is recovered. On this way those effects today related to structural changes were named in the literature memory effects: the electrochemical responses keep memory of the previous cathodic potential limit.[42-47]

Table 1 Structural processes originate different reaction rates (dQ/dV) on Figure 3c separated by the characteristic potentials: $E_1$, $E_2$, $E_3$, $E_4$ and $E_5$, which experience some evolution for different cathodic potential limits. Evolution of the charges for the closed (film redox processes) and open (irreversible reaction) parts of the coulovoltammetric (QV) responses from figure 3b.

| Cathodic potential limits / V | $E_1$ / V | $E_2$ / V | $E_3$ / V | $E_4$ / V | $E_5$ / V | Redox film Charge / C | Irreversible Charge / C |
|---|---|---|---|---|---|---|---|
| -0.6 | - | -0.48 | -0.28 | 0.62 | 0.25 | 0.13250 | -0.00307 |
| -1.0 | -0.78 | -0.60 | -0.3 | 0.61 | 0.35 | 0.18816 | -0.00201 |
| -1.2 | -0.81 | -0.60 | -0.16 | 0.60 | 0.38 | 0.19538 | -0.00072 |
| -1.5 | -0.84 | -0.60 | 0.17 | 0.60 | 0.48 | 0.19626 | 0.00288 |
| -1.7 | -0.8 | -0.60 | 0.12 | 0.59 | 0.54 | 0.19088 | 0.00725 |
| -2.0 | -0.8 | -0.60 | 0.18 | 0.58 | 0.56 | 0.18400 | 0.01610 |

For conducting polymers exchanging small anions the closed coulovoltammetric loop shows four structural slope changes related to: reduction-shrinking, reduction-compaction, oxidation-relaxation and oxidation-swelling processes.[31,41] Now six slope (Q/E) changes are observed (Figure 3c) which chemical and structural origin we will try to clarify here. Each of the abrupt slope variations indicates the characteristic potential ($E_1$, $E_2$, $E_3$, $E_4$ and $E_5$) of a structural change. Table 1 show those potentials and the charges related to each of the different structural parts (charge variation between two characteristic potentials).

### 3.3 Stationary Chronoamperometric Responses

Chronoamperometric responses, Figure 4a for the self-supported PPy-HpPS film oxidation and figure 4b for the film reduction, were obtained in 0.5M NaCl solution from the film submitted to consecutive square potential steps from different cathodic potentials, kept every time for 500s, to the same anodic potential of 0.7V also kept for 500s. The square potential step was repeated three times corroborating that after the second square wave any structural memory was erased getting stationary anodic and cathodic chronoamperometric responses.

a b

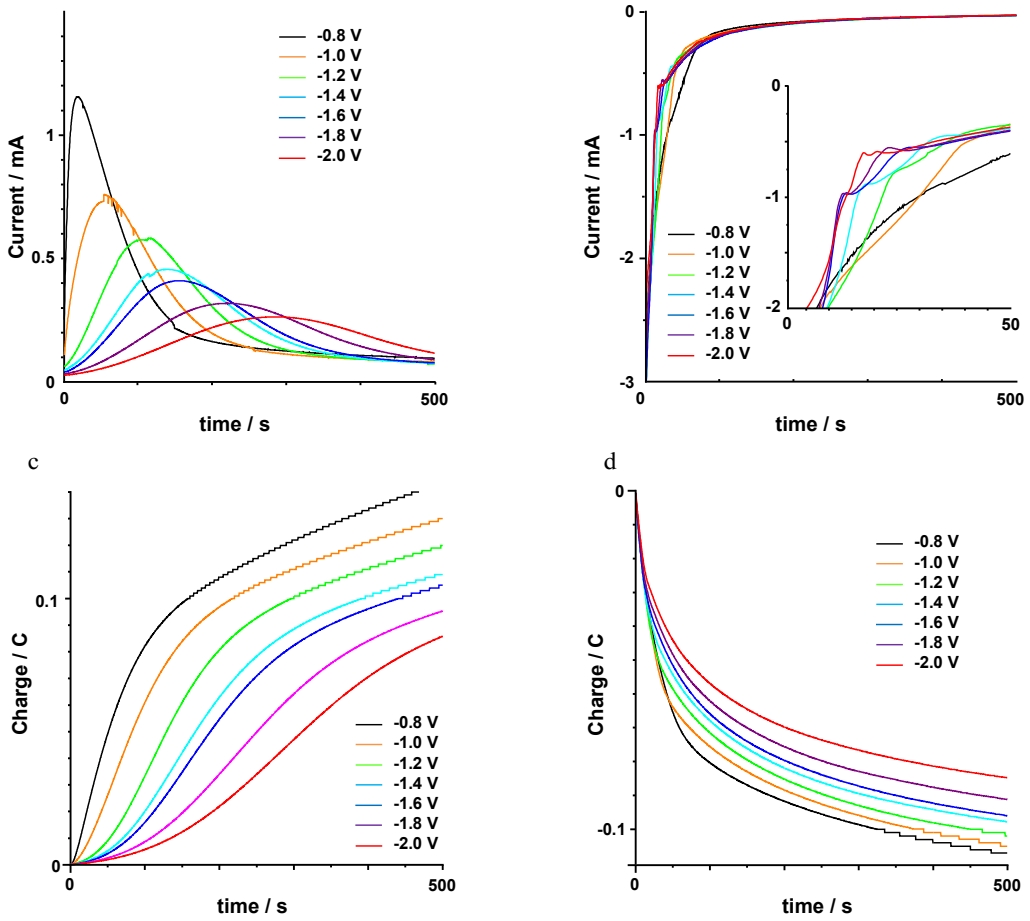


**Fig. 4** Chronoamperometric responses from the self-supported PPy-HpPS film in 0.5M NaCl solution, (a) film oxidation by potential steps from different cathodic potential limits (indicated on the figure), kept every time for 500s, to the same anodic potential limit of 0.7V also kept for 500s. (b) film reduction by potential step back to the studied cathodic potential. Evolution of charge consumed during (c) oxidation and (c) redution obtained by integration of the chronoamperometric responses (a) and (b).

The anodic chronoamperograms show a maximum that, according with the ESCR model, indicates that the more reduced states of the film, attained by polarization for the same time at rising cathodic potentials, are energetically most stable. The subsequent oxidation is initiated by nucleation-relaxation: the extraction of electrons from the chains and the parallel exchange of charge balance counteirons in the film only become possible at those points (nuclei) of the film where the chains have a greater mobility.[48] The nuclei growth promotes the increase of the current. The nuclei coalescence originates the current maximum. The sequence of the processes becomes slower (lower maxima at higher oxidation times) when more reduced and energetically stable structures are got by reduction at rising cathodic potentials for the same reduction time (Figure 4a).

After oxidation the PPy-HpPS film reduction responses present, figure 4b, a complex structure including two shoulders. A uniform reduction of the film under diffusion control (Cottrell chronoamperograms) of the counterions towards the solution should give a continuous decrease of the current The two shoulders in actual responses indicate the presence of two new (not described by the ESCR model) structural processes taking place in the film during reduction that can be induced by the presence of different ionic (anions, or cations) exchanges.

The attained oxidation and reduction responses correspond, from a chemical point of view, to the film oxidation and reduction kinetics defined by the flowing current, I, ($I = dq/dt$; and $dq/F = dn$, where n is the number of exchanged ions and F the Faraday's constant; so $I = dn/dt$; considering the mass, m, of the polymer film immersed in the electrolyte, $i = I/m = (1/m)dn/dt$, and this specific current (per unit of mass) i flowing by the material immersed in solution controls the variation of the counterion's specific concentration in the film per unit of time: the current control the specific film oxidation rate. By integration of figures 4a and b ($q = i\int dt$), figure 4c and 4d, respectively, were attained. The slope, at any time ($dq/dt = dn/dt$) represents the film reaction rate getting reactions having an induction time (S shape), characteristic of reaction inducing structural transformations, or allosteric effects in proteins.[10,49,50]

Figures 4c and 4d show lower initial reaction rates after film reduction at rising cathodic potentials. They illustrate a chemical paradox: deeper reduced initial states, got by reduction at rising cathodic potentials, give slower subsequent oxidation rates by potential step to the same oxidation potential.

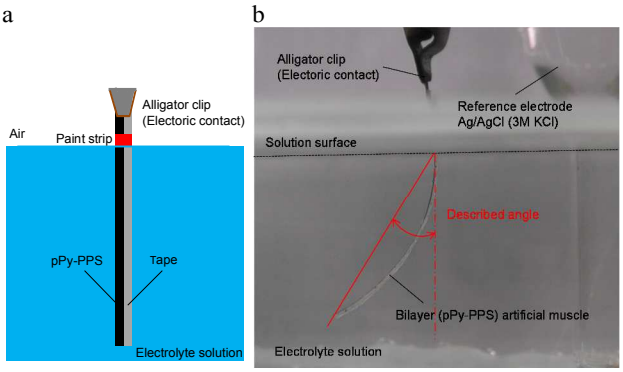


**Fig. 5** (a) Scheme of the pPy-HpPS/tape bilayer artificial muscle with the relative position of the two constitutive layers as in the checked muscles, transversal paint strip and alligator metal electric contact. (b) A picture of a PPy-HpPS/tape bilayer muscle in the cell and determination of the described angle.

After oxidation for the same time figures 4b and 4d indicate that some memory effect still remains affecting the subsequent reductions: lower reduction rates are obtained when the films were reduced at more cathodic potentials in the previous cycle. The film oxidation consumes (figure 4c) decreasing charges after oxidation for 500s and those partial oxidations don't erase the structural memory attained at the cathodic potentials.

As a partial conclusion both, coulovoltammetric and chronoamperometric responses point to the presence of complex structural transformations in the film and complex ionic exchanges between the film and the solution driven by the film's reactions. One of the best tools to transfer small amounts of ionic exchanges into macroscopic movements are bending bilayer, or triple layer, artificial muscles.[12,13] The bilayer muscles transduce small ionic exchanges (volume changes) in the PPy film into large bending angles in opposed directions: clockwise (+theta)/anticlockwise(-theta), depending on the relative position-PPy/Tape or Tape/PPy- of the bilayer) for anion/cation exchanges.[1-3]

### 3.4 Bending Bilayer (conducting polymer/tape) artificial muscle: macroscopic structural changes

A polymer (PPy-HpPS) film was electrogenerated on stainless steel and peeled off from the electrode and then it was rinsed several times with double distilled water and dried. Using a double side 3M tape a bilayer pPy-HpPS/tape was obtained. After uniform pressure of the tape (protected with a plastic ribbon) the pPy-HpPS bilayer was peeled off from the electrode and the protected plastic ribbon was removed. A transversal paint strip (between 2 mm and 5 mm below the bilayer top and surrounding the full bilayer) avoids the electrolyte ascension by capillarity (Figure 5a). The 2 mm of the top pPy film free of paint were used for the electrical connection, through a metal clamp, to the working electrode exit of the potentiostat-galvanostat. The bilayer muscle below the paint strip was immersed in the electrolyte (0.5 M NaCl aqueous solution) the meniscus below the paint strip. Figure 5b shows a picture of the bilayer PPy-HpPS/Tape muscle bending in the cell electrolyte under current flow. When the PPy-HpPS film swells due to entrance of ions and solvent driven by the electrochemical reaction an anticlockwise (-theta) bending movement is observed. When the film shrinks due to the reaction driven expulsion of ions and solvent clockwise (+theta) bending movements are observed. The movement of the artificial muscle during electrochemical experiments is recorded using a video camera correlating times, applied potential and frames.

By using a Stainless Steel plate as counter electrode and the reference electrode the muscle was submitted to consecutive potential sweeps from -1.0 V to 0.7 V at a scan rate of 10 mV $s^{-1}$ and room temperature. Figure 6a shows the stationary voltammetric response that, by integration, gives the stationary coulovoltammetric response shown by figure 6b. The parallel bending movements were video recorded. From the video frames the evolution of the angle described by the muscle bottom (determined as indicated by figure 5b) was followed as a function of the applied potential, Figure 6c. The points (1), (2), (3) and (4) on the coulovoltammogram (Fig 6b) correlate with the angles on Fig 6c and pictures of the muscles and schemes on Figure 6d.

Starting from -1.0 V and following the anodic potential sweep the muscle reduces (fig 6b, negative shift of the charge) and the actuator bends clockwise (fig 6c and pictures) up to the coulovoltammetric minimum, point (1): the PPy-HpPS film swells by reduction in that potential range. From (1) to (2) a fast oxidation (positive shift of the charge) occurs (fig 6b) promoting an anticlockwise (fig 6c and pictures) bending movement: the PPy film shrinks by oxidation from (1) to (2). From (2) to (3) the oxidation rate is slower (fig 6b) giving a clockwise movement (fig 6c and pictures): the PPy-HpPS film swells by oxidation from (2) to (3). From (3) to (4) a slow reduction takes place while the muscle bends anticlockwise: the PPy-HpPS film shrinks by reduction from (3) to (4). Finally from (4) to (1) the film reduces very fast at the beginning and slowly later on while the muscle always bends clockwise: the PPy-HpPS film swells from (3) to (4). The bending movement is not fully reversible presenting some clockwise creeping effect (shrinking). The amplitude of the movement [difference between the minimum-(1)-and the maximum-(4)-angle] was 28 degrees. The creeping effect was clockwise 6 degrees.

The muscle also was checked in 0.5 M $NaPF_6$ aqueous solution. Figures (7a, b, c and d) show the voltammetric, coulovoltammetric, bending responses and pictures, respectively. The system presents a minor irreversible reaction detected and quantified by the charge of the open Q/V part (Fig. 7b) at the most cathodic potentials. The closed part of the loop, related to the reversible redox processes in the film involves most of the charge. The oxidation charge, from (1) to (3) in Fig 7(b) originates an anticlockwise movement of the muscles: the PPy-HpPS film swells. The reduction charge from (3) to (1)

a b c

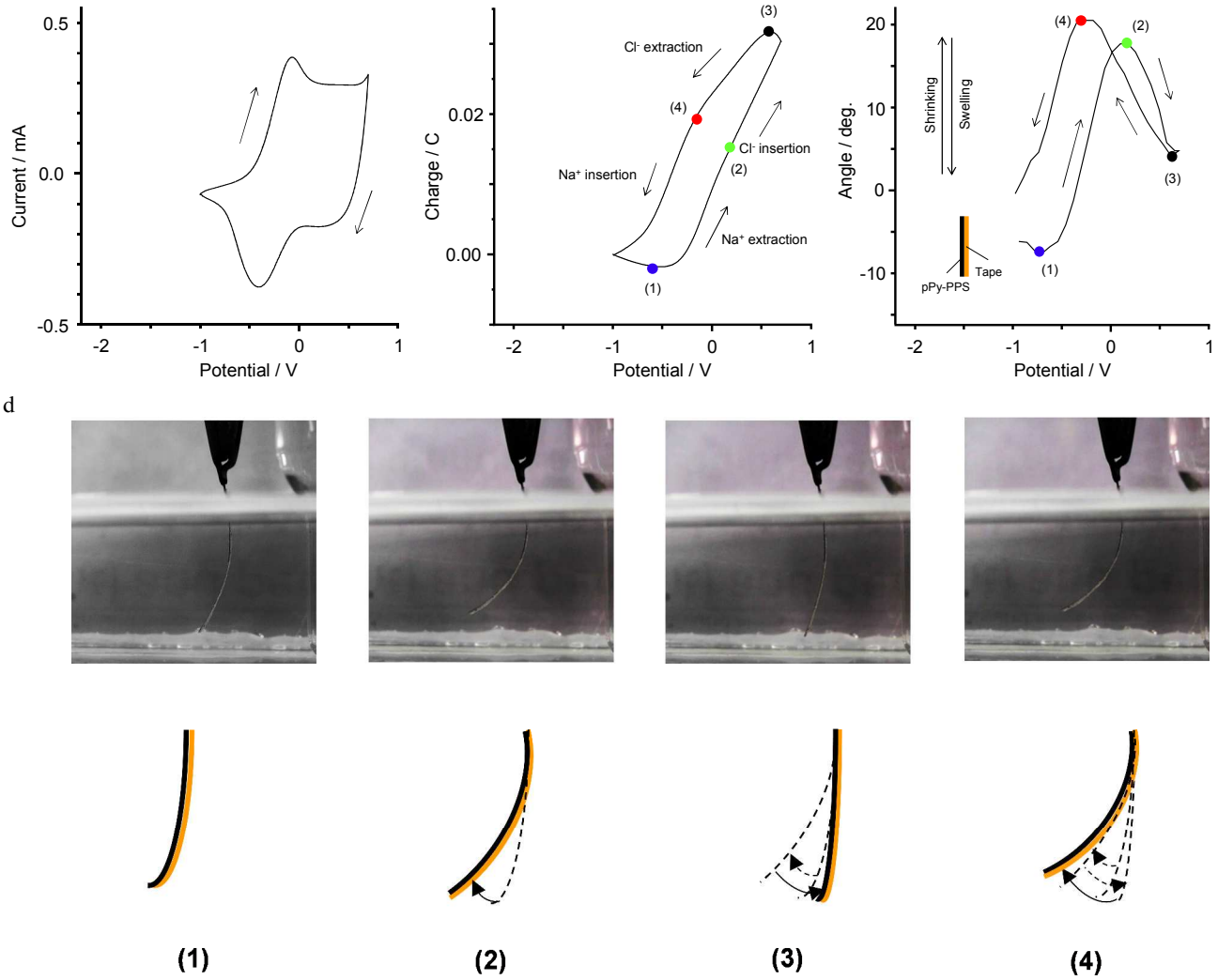


**Fig. 6** The PPy-HpPS/tape artificial muscle was submitted to consecutive potential sweeps from -1.0 V to 0.7.0 V and the same anodic potential limit of 0.7 V, at 10 mV $s^{-1}$ in 0.5 M NaCl aqueous solution. (a) Stationary voltammetric response, (b) Parallel coulovoltammogram (c) Evolution of the angle described (Fig 5b) with the potential. (d) Lateral pictures of the bilayer muscle obtained at the points 1, 2, 3 and 4 from figures 6b and 6c during the potential cycle and their pattern diagrams, at the same points, (left side, PPy-HpPS film/ right side, tape: PPy swelling/shrinking gives anticlockwise/clockwise bending).

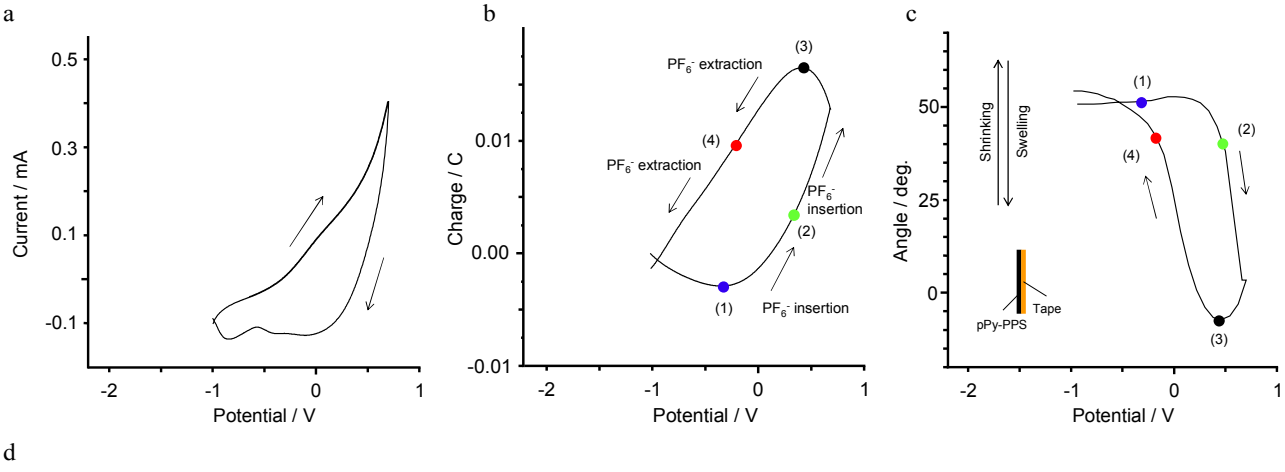

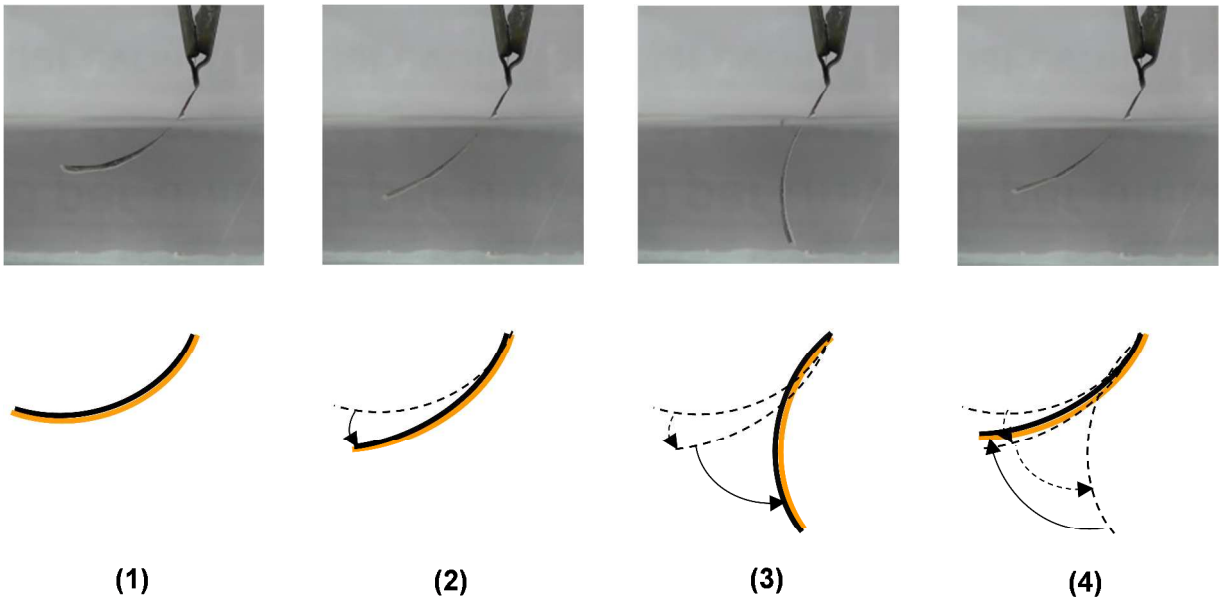


**Fig. 7** The PPy-HpPS/tape artificial muscle was submitted to consecutive potential sweeps from -1.0 V to 0.7.0 V and the same anodic potential limit of 0.7 V, at 10 mV $s^{-1}$ in 0.5 M $NaPF_6$ aqueous solution. (a) Stationary voltammogram, (b) Parallel coulovoltammetric response, (c) Angle described as a function of the muscle potential. (d) Lateral pictures of the bilayer muscle obtained at the points 1, 2, 3 and 4 from figures 7b and 7c during the potential cycle and their pattern diagrams, at the same points, (left side, PPy-HpPS film/ right side, tape: PPy swelling/shrinking gives anticlockwise/clockwise bending).

(fig. 7b) drives a clockwise movement (fig 7c and pictures): the PPy film shrinks. The described angle during the voltammetric cycle is 61 degrees (54+7), over two times the amplitude of the movement (28 degrees) attained per cycle in NaCl aqueous solutions (Figure 6c). A creeping anticlockwise effect of 4 degrees was observed.

### 3.5 EDX analysis of the films under different oxidation states

Figure 8(a) and 8(b) show the EDX (Energy Dispersive X-ray spectroscopy) results of self-supported films of PPy-HpPS after signal at 2.61 keV [Figure 8a, inset line (3)] showing the maximum concentration in the full-oxidized film. The chlorine concentration decreases for rising reduced films [line (4)] being still present, in a low concentration, in the reduced film [line (1)].

From the film oxidized in NaPF6 aqueous solution, two clear fluorine signals are observed at 0.67 and 0.68 keV (Fig. 8b inset) being present in the oxidized film [point (3), 0.43 mV] or in the films reduced until point (4), -0.24 V. The phosphorus also gives two signals at 2.00 and 2.01 keV (Fig. 8b inset) being present in the oxidized film [point (3), 0.43 V] and in the films reduced until point (4), -0.24 V. The signal them decreases for deeper reduced [point (1), -0.33 V] states.
The HpPS content, as NapPS and HpPS, remains constant, according with the S content that gives a signal at 2.3keV, for the different studied oxidation states [Figs 8a and 8b, insets].

### 3.6 Ionic content variations, muscle movements and film reactions

According with the EDX analysis, the coulovoltammetric responses and the bending movements the PPy-HpPS film follows in NaCl a prevalent entrance of $Na^+$ by reduction from voltammetric cycling in NaCl or $NaPF_6$ aqueous solution, respectively. The last cathodic sweep was stopped at a different potential every time, corresponding to the coulovoltammetric minimum (1), the coulovoltammetric maximum (3) and the intermediate reduction state (4) stated in figures 6b and 7b.

From the film oxidized in NaCl aqueous solution the **sodium** gives a signal at 1.05 keV (Fig. 8a inset) being present only in the full-reduced film [point (1), –0.62V]. The Na is absent in both, the oxidized film [point (3), 0.59 V] or in the films reduced until -0.18 V, point (4). The **chlorine** gives a (4) to (1) and the $Na^+$ expelling by oxidation from (1) to (2) (Fig 6). The driving reversible electrochemical reaction can be written as:

$$PPy(N_aPPS)_n\,(H_2O)_o \underset{red}{\overset{ox}{\rightleftharpoons}} PPy^{n+}(pPS^-)_n + o(H_2O) + nNa^+ + ne^- \qquad (1)$$

During the oxidation from (1) to (2) the forwards reaction promotes the expulsion of $Na^+$ (Fig 8a, inset) with the subsequent film shrinking (Fig 6c). During the film reduction from (4) to (1), (reaction 1 backwards) the sodium insertion prevails (Fig 8a, inset) driving the film swelling (Fig 6c).

The PPy-HpPS film follows a prevalent exchange of anions (Fig 8a) with $Cl^-$ insertion and film swelling (Fig 6c) by oxidation from (2) to (3) and expulsion of $Cl^-$ (Fig 18a), and the film shrinks (Fig 6c) by reduction from (3) to (4). The driving reversible electrochemical reactions can be written as:

$$PPy^{m+}(HpPS)_n\,(Cl^-)_m + n(Cl^-)_{solv} + oH_2O \underset{red}{\overset{ox}{\rightleftharpoons}} PPy^{(m+n)+}(HpPS)_n\,(Cl^-)_{(m+n)}(H_2O)_o + ne^- \qquad (2)$$

The $Cl^-$ insertion prevails, driven by the polymer oxidation (reaction 2 forwards) from (2) to (3) promoting the swelling of the film (Fig 6c). The $Cl^-$ expulsion prevails, driven by the polymer reduction (reaction 2 backwards) from (3) to (4). According with the EDX results the $Cl^-$ expulsion goes on up to a

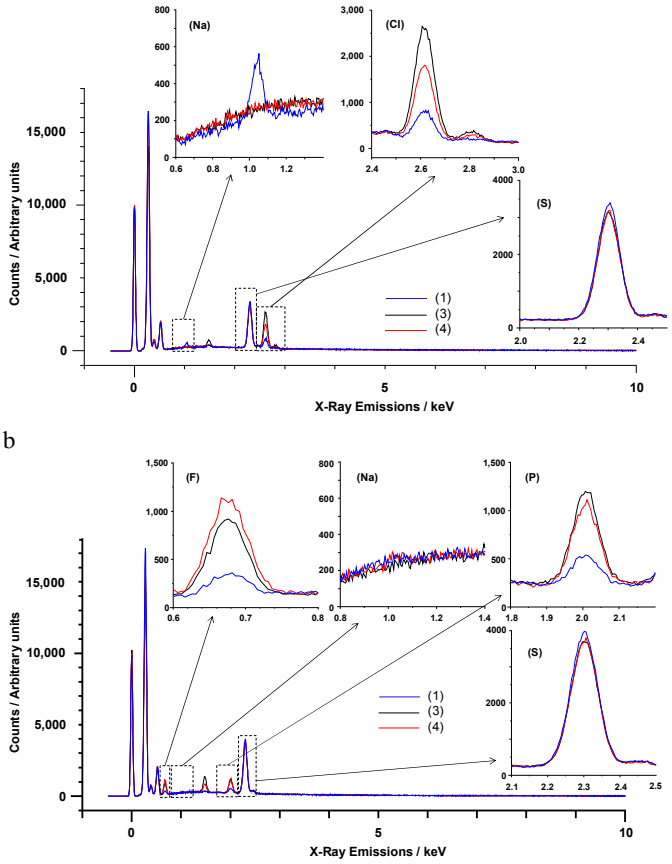


**Fig. 8** (a) EDX spectra from three free-standing PPy-HpPS films after ten consecutive voltammetric cycles between -1.0V and 0.7V in 0.5 M NaCl aqueous solution at 10 $mVs^{-1}$: the ten cycle was stopped at 0.59 V(coulovoltammetric maximum) black line; -0.18 V(intermediate reduction), red line; or -0.57 V (coulovoltammetric minimum) blue line for each of three different films. (b) EDX spectra from three free-standing PPy-HpPS films after ten consecutive voltammetric cycles between -1.0V and 0.7V in 0.5 M $NaPF_6$ aqueous solution at 10 $mVs^{-1}$: the ten cycle was stopped at 0.43 V, black line (coulovoltammetric maximum), -0.24 V, red line (intermediate reduction) or -0.33 V, blue line (coulovoltammetric minimum), for each of three different films.

the cathodic potential limit and still a high fraction (31%) remains in the film at this potential. Those facts point to the formation of a very stable, from an energetic point of view, $PPy^{(m+n)+}$ $(HpPS)_n$ $(Cl^-)_{(m+n)}(H_2O)_o$ compound that requires high cathodic overpotentials and time to be reduced. This ionic exchange fits those found in PPy films with small anions. [13,14]

Thus, despite that the materials was generated in presence of a large excess of HpPS a fraction of the film electroactive PPy ($Q_{Cl}$/ $Q_{Cl}$ +$Q_{Na}$) requires $Cl^-$ anions to compensate the new positive charges generated on the PPy chains indicating that the pPSH present in the film doesn't dissociate to $pPS^-$ despite the high applied anodic potentials. It is expected that, even if the dissociation constant of this acid is very small some of the acid could be dissociated at those high anodic potentials participating in the PPy oxidation completion:

$$PPy\text{-}pPSH + o(H_2O)_o \underset{red}{\overset{ox}{\rightleftharpoons}} PPy^{n+}(pPS^-)_n(H_2O)_o + nH^+ + ne^- \quad (3)$$

In order to check this hypothesis a self-supported PPy-HpPS film was deep reduced and oxidized in NaCl aqueous solution containing a drop of methyl-orange (pH indicator, red at pH< 3.2 and yellow at pH>4.4) by consecutive potential steps from -1.5V to 0.7V, each kept for 300s. Figure 9a show the chronoamperometric responses. Pictures from figures 9b and 9c show both, electrode and electrolyte at the end of the reduction step and after 180 s of anodic polarization. A red cloud is formed around the electrode after oxidation at 0.7V for 180 seconds, rising through the electrolyte towards its surface (Figure 9c) corroborating the acidification of the solution around the electrode, according with the film reaction 3.

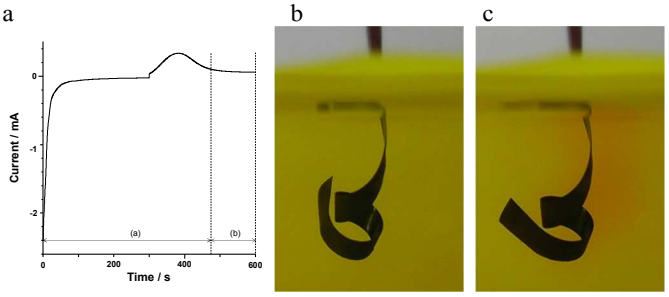


**Fig. 9** (a) Chronoamperometric responses from a self-supported PPy-HpPS film submitted to -1.0V and 0.7V kept every time for 300s in 0.5M NaCl solution containing one drop of a 0.1% methyl orange aqueous solution (b) film and solution picture at the end of the cathodic (reduction) polarization (c) picture after oxidation at 0.7V for 180 sec (a red cloud is formed around the electrode rising towards the surface).

The results from the film treated in $NaPF_6$ indicate the entrance of the $PF_6^-$ during the film oxidation from (1) to (3) (fig. 7b) and its expulsion from (3) to (4) (where around 32 % of the ions still remains in the film) during the films reduction. The driving reversible electrochemical reactions can be written as:

$$(PPy^{m+})(PF_6^-)_m + n(PF_6^-)_{solv} + oH_2O \underset{red}{\overset{ox}{\rightleftharpoons}} (PPy^{(m+n)+})(PF_6^-)_{(m+n)}(H_2O)_o + ne^- \quad (4)$$

So, during oxidation (reaction 3 forwards) the film swells (Figure 7c) and the reduction (reaction 3 backwards) drives the film shrinking (Figure 7c).

When the HpPS concentration inside the film is high enough the slow irreversible hydrogen evolution:

$$2HpPS + 2Na^+ + 2e^- \rightarrow 2NapPS + H_2 \quad (5)$$

takes place at cathodic potentials in any of the studied electrolytes giving an open part of the coulovoltammetric response (Figures 3b and 3c).

The film composition in NaCl aqueous solutions is governed by reactions 1, 2, 3 and 5.

From the results obtained in NaCl aqueous solutions we can conclude that the film after oxidation up to 0.59V, point (3) from figure 6b, contains: $[PPy^{n+}(PSS^-)_n]$ originated by reaction 1 forwards, $[(PPy^{(m+n)+}\ (Cl^-)_{(m+n)}]$ produced by reaction 2 forwards, $PPy^{n+}\ (pPS^-)_n$ reaction 3 forwards, pPSH excess present in the full potential range and the water required for the ions solvation and the polymer hydration (osmotic pressure).

At the intermediate redox state represented by point (4), -0.18V, in figure 6b, the film composition includes: $[PPy^{n+}(PSS^-)_n]$ originated by reaction 1 forwards, $[(PPy^{m+}\ (Cl^-)_m]$ originated by reaction 2 backwards; and pPSH (reaction 4 backwards and excess content) and the water required for the ions solvation and osmotic balance.

The sample reduced up to -0.6V, point (1) in fig. 6b, is constituted by: some water required for the ions solvation and osmotic balance; $PPy(N_apPS)_n$ originated by reaction 1 backwards, $[(PPy^{p+}\ (Cl^-)_p]$ produced by reaction 2 backward that goes on during the full potential sweep, and HpPS, reaction 3 backwards and excess content. At more cathodic potentials that -1.0V the slow irreversible hydrogen evolution starts increasing the content of (NapPS) originated by reaction 4 in the reduced film.

In $NaPF_6$ solutions the film compositions are simplest being mainly governed by reactions 4 and 5.The film oxidized up to the point (3) in figure 7b (0.43V ) is mainly constituted by: $[(PPy^{n+})(PF_6^-)_n]$ originated by reaction 4, excess of HpPS and the water required for the ions solvation and osmotic balance. The film reduced until point (1) in figure 7b (-0.33V) is constituted by: PPy originated by reaction 4 backwards, excess of HpPS and the water. For more cathodic potential limits than -0.9V reactions 4 (backwards) and 5 coexist increasing the (HpPS) content.

### 3.7 Description of the voltammetric, culovoltammetric and chronoamperometric responses by the driving reactions and structural changes

The electrochemical results could now be explained as a function of the film reactions prevailing in the different potential ranges and driving the different ionic exchanges.

Voltammetric and coulovoltammetric results from $NaPF_6$ aqueous solutions correspond to a prevalent exchange of anions during the oxidation/reduction reaction in the full studied potential range, reaction 3: the polymer swells by oxidation, shrinks and compact its conformational structure by reduction. The HpPS present in the film doesn't play any mayor role in the ionic exchange only controlling the irreversible hydrogen release at the more cathodic potential limits.

The coulovoltammetric results (Fig 3c and 6b) from NaCl aqueous solutions indicate that the $Na^+$ exchange takes place at the more cathodic potential region and the $Cl^-$ exchange prevails at the more anodic potentials but coexisting (as a minor exchange) during the prevalent $Na^+$ exchange. During reduction $E_3$ defines the transition from a mayor $Cl^-$ expulsion (indicated as $-Cl^-$) and film shrinking (Reaction 2, backwards) to a mayor $Na^+$ entrance (indicated as $+Na^+$) and film expansion (Reaction 1 backwards): from now on the potential $E_3$ will be nominated $E_{-Cl/+Na}$, $E_5$ becoming $E_{-\ Na\ /+Cl}$. From this potential the fast $Na^+$ entrance (high Q/E slope) goes on driven by reaction 1 backwards up to $E_1$ where a slow $Na^+$ entrance occurs, driven by the same reaction but generating of a new energetically stable structure of $[(NapPS)_n(H_2O\ )_o]$. This structural change overlaps the slow transformation of HpPS into NapPS with a parallel irreversible discharge of protons. Whether the parallel HpPS transformation and hydrogen evolution participates, or not, in the structural energetic change of the $[(NapPS)_n(H_2O\ )_o]$ remains as a pending point. From now on $E_1$ will be named as $E_{ES}$ due to the **energetic structural** change there initiated. $E_2$ is the potential for the beginning of the material oxidation with entrance of $Na^+$: when the film is reduced up to more cathodic potential limits than $E_{ES}$ the subsequent **oxidation** begins under nucleation/**relaxation** control from now it will be $E_{OR(+Na)}$. At $E_4$ the nucleation/relaxation is finished and the oxidation/swelling with entrance of $Na^+$ goes on, from now $E_4$ it will be named $E_{+Na}$.

Rising amounts of the new energetically stable reduced and swollen $[PPy(N_apPS)_n(H_2O\ )_o]$ structure generated at more cathodic potential limits than $E_2$ promote the anodic shift of both, the oxidation potential (Fig. 3a) and the oxidation maximum on the subsequent anodic voltammetric responses: more energy is required to break, initiated by a nucleation process, this stable structure. The only source, working under constant temperature (constant thermal energy) and electrolyte concentration (constant chemical energy) is the electrochemical energy (the anodic overpotential): the beginning of the material oxidation shifts to more anodic potentials for materials reduced up to more cathodic potentials where more stable reduced structures were attained.

They also induce the decrease of the oxidation-nucleation maxima and its shift towards higher oxidation times on the anodic chronoamperometric responses (Fig 4a): under constant chemical and electrical energetic conditions (constant: temperature, electrolyte concentration and anodic overpotential) breaking more stable structures, initiated by nucleation-relaxation, occurs at lower reaction rates (lower currents) requiring longer oxidation times. The above mentioned electrochemical paradox of the chronoamperometric responses (lower oxidation rates from more reduced films) becomes now clarified: more stable reduced states attained by reduction at rising cathodic potentials give, when used as initial states for the oxidation under constant energetic conditions, slower oxidation reactions.

The physical nature of this stable reduced structure will require an ulterior study.

Once the $[PPy(NapPS)(H_2O\ )_o]$ was oxidized, shrunk and packed between $E_{OR(+Na)}$ and $E_{+Na}$ (Fig. 3c), a fraction of the PPy remains reduced and a slow oxidation with entrance of $Cl^-$ ions (reaction 2 forwards) is initiated: the polymer swells again (Fig 6c) up to the end of the potential sweep. Reactions 2 forwards and 2 backwards are slower than the previous expulsion of $Na^+$ (Figs 3c and. 5b). The HpPS also participates

(reaction 4) with the film acidification (Fig 9c) in this potential range.

Table 2 Charges consumed during of the structural processes (Fig. 3c) separated by the characteristic potential from Table 1for the different cathodic potential limits shown by fig. 3b: $-Q_{sh\text{-}Cl\text{-}}$ reduction charge inducing film shrinking and $Cl^-$ expulsion from the QV maximum to $E_3$; $-Q_{sw+Na+}$ reduction charge inducing film swelling by entrance of $Na^+$ from $E_3$ to $E_1$; $-Q_{sw+Na+ses}$ reduction charge giving film swelling by $Na^+$ entrance and film reorganization towards an stable energetic structure (ses); $Q_{irr}$, irreversible hydrogen evolution (reaction 5); $Q_{sh\text{-}Na+}$ oxidation charge inducing $Na^+$ expulsion and film shrinking from $E_4$ to $E_5$; $Q_{sw+Cl\text{-}}$ oxidation charge giving $Cl^-$ entrance and film swelling from $E_5$ to the QV maximum.

| Cathodic potential limits / V | $-Q_{sh\text{-}Cl\text{-}}$ / C | $-Q_{sw+Na+}$ / C | $-Q_{sw+Na+ses}$ / C | $-Q_{irr}$ / C | $Q_{sh\text{-}Na+}$ / C | $Q_{sw+Cl\text{-}}$ / C |
|---|---|---|---|---|---|---|
| -0.6 | 0.082 | 0.045 | - | -0.0030 | 0.045 | 0.082 |
| -1.0 | 0.095 | 0.075 | 0.015 | -0.0020 | 0.119 | 0.066 |
| -1.2 | 0.109 | 0.073 | 0.013 | 0.0007 | 0.143 | 0.052 |
| -1.5 | 0.118 | 0.066 | 0.012 | 0.0029 | 0.157 | 0.039 |
| -1.7 | 0.114 | 0.006 | 0.017 | 0.0070 | 0.164 | 0.027 |
| -2.0 | 0.106 | 0.064 | 0.014 | 0.0160 | 0.184 | - |

As deduced from figure 3c the different potential domains correspond to structural changes (swelling, shrinking, compaction, formation of stable structures) induced by the reactions and consuming the charge differences between the beginning and the end of every potential range. From the maximum to $E_3$ the polymer reduces and shrinks by expulsion of $Cl^-$ (**shrinks -$Cl^-$**) consuming the charge $-Q_{sh\text{-}Cl\text{-}}$ (negative increment is a reduction charge). From $E_3$ to $E_1$ the polymer reduces and swells by $N_a^+$ entrance (**swells +$Na^+$**) consuming the charge $-Q_{sw+Na+}$. From $E_1$ to $E_2$ the polymer reduces, swells by $N_a^+$ entrance and reorganizes giving a stable energetic structure (**swells +$Na^+$ + stable energetic structure**) consuming the charge $-Q_{sw+Na+ses}$. Overlapping this process an **irreversible hydrogen evolution** occurs consuming the charge $-Q_{irr}$. From $E_4$ to $E_5$ the polymer shrinks by oxidation with $Na^+$ expulsion (**shrinks -$Na^+$**) consuming the charge $Q_{sh\text{-}Na+}$. From $E_5$ to the coulovoltammetric maximum the polymer swells by oxidation with $Cl^-$ entrance (**Swells +$Cl^-$**) consuming the charge $Q_{sw+Cl\text{-}}$. The evolution of those structural charges as a function of the cathodic potential limits is presented by table 2.

## Conclusions

Thick films of PPy-HpPS were electrogenerated on stainless steel electrodes from aqueous solutions and peeled off from the metal to be used as both, self-supported film electrodes or as PPy-HpPS/tape bilayer artificial muscles.

The HpPS was elected because it is a small organic acid which PPy blend can originate complex ionic exchanges during electrochemical control.

The voltammetric, coulovoltammetric and chronoamperometric responses from the self-supported film in NaCl aqueous solutions indicate, and the bending muscle corroborates, the presence of complex ionic exchanges. The concomitant structural transformations to energetically stable states at more cathodic potential than –0.8V (deep reduced and swollen state) and at more anodic potentials than 0.25 to 0.56V (more oxidized and swollen states). Shrunk states were obtained for an intermediate oxidation potential range (from -0.42mV to 0.50V).

In $NaPF_6$ aqueous solution, the electrochemical responses indicate, and the bending muscle corroborates, that the film shrinks, closes and compact its structure by reduction; relaxing and swelling by oxidation. Those reaction driven structural changes are described by the ESCR model for pPy films exchanging only anions.

The EDX analysis of films, each oxidized at a different potential, indicate a high and constant pPS content (as $pPS^-$, NapPS or HpPS) whatever the oxidation state of the film in every studied electrolytes. The HpPS promotes a very slow irreversible hydrogen evolution at more cathodic potentials than -1.2V (reaction 5) and the release of protons from the film at more anodic potentials than 0.7V (reaction 3).

In $NaPF_6$ the oxidized/reduced films contains a high/low, respectively, concentration of $PF_6$, the cation $Na^+$ being absent in both estates. Ionic exchanges, film volume variations and structural changes on the electrochemical responses indicate that reaction 4 drives ionic exchanges and structural or volume variations.

In NaCl the $Na^+$ exchange prevails during reduction (entrance during reduction and exit during oxidation) driven by reaction 1. Once the $Na^+$ was expelled from the film the entrance of $Cl^-$ prevails at the most anodic potential limits driven by reaction 2. The minor expulsion of $Cl^-$ during reduction goes on during the prevalent $Na^+$ entrance.

The double ionic exchange in NaCl ($Na^+$ expulsion followed by $Cl^-$ entrance) induces anticlockwise followed by clockwise bending movements of the PPy-HpPS muscle during voltammetric oxidation. In $NaPF_6$ only the anion entrance compensates the PPy positive charges generated by oxidation and the amplitude of the muscle bending movement is 61 degrees, over two times the amplitude got in NaCl (28 degrees).

Based on the driving reactions a chemical composition is proposed for the film at each of the characteristic potentials in the two studied electrolytes.

The described methodology could be translated to quantify similar problems in biological reactions giving health or illnesses.

## Acknowledgements

The authors acknowledge the financial support from the Kyushu Institute of Technology and the Spanish Government (MCINN) Projects MAT2011-24973.

## Notes and references

[a]Kyushu Institute of Technology, Department of Mechanical Information Science and Technology, 680-4 Kawazu, Iizuka, Fukuoka, 820-8502, (Japan).

[b]Center for Electrochemistry and Intelligent Materials, Universidad Politécnica de Cartagena, AularioII, Paseo Alfonso XIII, E-30203, Cartagena, Murcia, (Spain).

1. T. F. Otero and J. G. Martinez, *J. Mater. Chem. B*, **2013**, 1, 26-38.
2. T. F. Otero, *Polym. Rev.*, **2013**, 53, 311-351.
3. T. F. Otero, J. G. Martinez and Arias-Pardilla *J. Electrochim. Acta*, **2012**, 84, 112-118.
4. G. Han, G. Shi, *Sensors and Actuators, B,* **2004,** 99, 525-531
5. G. Han, G. Shi, *J. Electroanal. Chem.*, **2004,** 569, 169-174
6. J. G. Martinez and T. F. Otero, *J. Phys. Chem. B*, **2012**, 116, 9223-9230.
7. T. F. Otero, J. J. Sanchez and J. G. Martinez, *J. Phys. Chem. B*, **2012**, 116, 5279-5290.
8. T. F. Otero, *J. Mater. Chem. B*, **2013**, 1, 3754-3767.
9. T. F. Otero and J. G. Martinez, *Adv. Funct. Mater.*, **2013**, 23, 404-416.
10. A. Fersht, *Enzyme Structure and Mechanism*, San Francisco: W. H. Freeman and Company (**1977**).
11. J. M. Hu, G. Q. Zhang, and S. Y. Liu, *Chem. Soc. Rev.*, **2012**, 41, 5933-5949.
12. T. F. Otero and J. G. Martínez, *Chem. Mater.*, **2012**, 24, 93-4099.
13. T. F. Otero, J. G. Martínez and B. Zaifoglu, *Smart Mater. Struct.*, **2013**, 22, 104019.
14. J. J. L. Cascales, A. F. Fernandez and T. F. Otero, *J. Phys. Chem. B,* **2003**, 107, 9339-9343.
15. J. J. L. Cascales and T. F. Otero, *Macromol. Theor. Simul.*, **2005**, 14, 40-48.
16. S. D. Oliveira Costa and J. J. L. Cascales, *Electroanal. Chem.*, **2010**, 644, 13-19.
17. C. Gabrielli, M. Keddam N. Nadi and H. Perrot, *J. Electroanal. Chem.*, **2000**, 485, 101-103.
18. C. Deslouis, T. El Moustafid, M. M. Musiani and B. Tribollet, *Electrochim. Acta*, **1996**, 41, 1343-1349.
19. C. Deslouis, M. M. Musiani, B. Tribollet and M. A. Vorotyntsev, *J. Electrochem. Soc.*, **1995**, 142, 1902-1908.
20. G. Lang and G. Inzelt, *Electrochim. Acta*, **1999**, 44, 2037-2051.
21. M. A. Vorotyntsev, C. Deslouis, M. M. Musiani, B. Tribollet and K. Aoki, *Electrochim. Acta*, **1999**, 44, 2105-2115.
22. M. F. Mathias, O. Haas, *J. Phys. Chem.*, **1993**, 97, 9217-9225.
23. A. R. Hillman and M. A. Mohamoud, *Electrochim. Acta*, **2006**, 51, 6018-6024.
24. M. J. M. Jafeen, M. A. Careem and S. Skaarup, *J. Solid State Electr.*, **2012**, 16, 1753-1759.
25. W. Plieth, A. Bund, U. Rammelt, S. Neudeck and L. M. Duc, *Electrochim. Acta*, **2006**, 51, 2366-2372.
26. S. Skaarup, M. J. M. Jafeen and M. A. Careem, *Solid State Ion.*, **2010**, 181, 1245-1250.
27. C. Visy, C. Janaky and E. Krivan, *J. Solid State Electr.*, **2005**, 9, 330-336.
28. A. R. Hillman and A. Robert, *J. Solid State Electr.*, **2011**, 15, 1647-1660
29. G. A. Snook, P. Kao and A. S. Best, *J. Power Sources*, **2011**, 196, 1-12
30. J. Heinze, B. A. Frontana-Uribe and S. Ludwigs, *Chem. Rev.*, **2010**, 110, 4724-4771.
31. T. F. Otero, M. Alfaro, V. Martinez, M. A. Perez and J. G. Martinez, *Adv. Funct. Mater.*, **2013**, 23, 3929-3940.
32. T. F. Otero, J. G. Martinez, M. Fuchiwaki and L. Valero, *Adv. Funct. Mater.*, **2014**, DOI: 10.1002/adfm.201302469.
33. T. F. Otero and J. G. Martínez, *Adv. Funct. Mater.*, **2013**, DOI: 10.1002/adfm.201302514.
34. L. V. Conzuelo, J. Arias-Pardilla, J. V. Cauich-Rodríguez, M. A. Smit and T. F. Otero, *Sensors 10*, **2010**, 2638-2374.
35. Y. Wu, G. Alici, G. M. Spinks and G. G. Wallace, *Synth. Met.*, **2006**, 156, 1017-1022.
36. A. Kaynak, C. Yang, Y. C. Lim and A. Kouzani, *Mater. Chem. Phys.*, **2011**, 125, 113–117.
37. M. S. Kang, Y. J. Choi, I. J. Choi, T. H. Yoon and S. H. Moon, *J. Memb. Scie.*, **2003**, 216, 39-53.
38. T. Sata, T. Sata and W. K. Yang, *J. Memb. Scie.*, **2002**, 206, 31-60.
39. R. M. Latonen, M. N. Akieh, K. Vavra, J. Bobacka and A. Ivaska, *Electroanalysis*, **2013**, 25, 991-1004.
40. T. F. Otero, H. Grande and J. Rodriguez, *Synth. Met.*, **1997**, 85, 1077-1078.
41. H. Grande and T. F. Otero, *J. Phys. Chem. B*, **1998**, 102, 7535-7540
42. T. F. Otero and E. Angulo, *Solid State Ionics*, **1993**, 63, 803-809.
43. C. Odin and M. Nechtschein, *Synth. Met.,* **1993**, 55, 1281-1286.
44. C. Odin and M. Nechtschein, *Synth. Met.*, **1993**, 55, 1287-1292.
45. C. Odin and M. Nechtschein, *Phys. Rev.*, **1991**, 67, 1114-1117
46. G. Inzelt, G. Horanyi and J. Q. Chambers, *Electrochim. Acta*, **1987**, 32, 757-763.
47. G. Inzelt, R. W. Day, J. F. Kinstle and J. Q. Chambers, *J. Phys.Chem.*, **1983**, 87, 4592-4598.
48. T. F. Otero and I. Boyano, *Chem. Phys. Chem.,* **2003**, 4, 868-872.
49. T. Atwood, P. Campbell, H. Parish, T. Smith, J. Stirling, F. Vella, R. Cammack, Oxford Dictionary of Biochemistry and Molecular Biology, Oxford University Press, Oxford, **2006**
50. "Voltage Dependent Channels", http://nerve.bsd.uchicago.edu/med98b.htm#VolttageDependentChannels accessed **2012**



 